MHD Mixed Convection Stagnation-Point Flow of a Micropolar Fluid in a Porous Medium Towards a Heated Stretching Sheet with Thermal Radiation

Dulal Pal[a] and Sewli Chatterjee[b]

[a]*Visva-Bharati University*

Santiniketan, 731235 West Bengal, India

[b]*Bengal Institute of Technology and Management (BITM)*

Santiniketan, 731236 West Bengal, India

E-mail(*corresp.*): `dulalp123@rediffmail.com`

E-mail: `sewlichatterjee@rediffmail.com`

Abstract. The present investigation is concerned with the study of heat and mass transfer characteristics on MHD boundary layer flow of an electrically conducting micropolar fluid over a non-isothermal stretching sheet embedded in a porous medium of variable thermal conductivity by applying prescribed heat flux for the heating processes. The thermal boundary layer equation takes into account of Ohmic dissipation due to transverse magnetic and electric fields. The governing system of partial differential equations is transformed into a system of non-linear ordinary differential equations using similarity transformation. The transformed non-linear coupled differential equations are linearized by quasi-linearization method and then solved very efficiently by finite-difference method. Attention has been focused to study the effects of various physical parameters on velocity, temperature and concentration in the boundary layer. Numerical data for the local skin friction coefficient, surface temperature and surface solutal concentration have also been tabulated for various parametric conditions.

Keywords: mass transfer, porous medium, magnetohydrodynamics, boundary layer flow, convection.

AMS Subject Classification: 34B15; 65L10; 76E06; 76W05; 80A20.

1 Introduction

The study of a non-Newtonian fluid flow due to a stretching surface is important in several engineering and industrial applications such as in the extrusion of a polymer sheet from a die, the drawing of plastic films and heat-treated materials travelling between a feed roll and a wind-up roll or materials man-

ufactured by extrusion, glass-fiber and paper production, cooling of metallic sheets, crystal growing and many others. In all these cases, the final products depend on the rate of cooling during stretching of the sheet. During manufacturing of these sheets, the mixture after passing from a slit is stretched in order to achieve the desired thickness. The final quality of such a sheet is influenced by heat and mass transfer between the sheet and the fluid. The heat and mass transfer of viscous fluids over an isothermal stretching sheet with suction or blowing have been studied by Gupta and Gupta [17]. Rahman [35] provided combined effects of internal heat generation and higher order chemical reaction on the non-Darcian forced convective flow of a viscous incompressible fluid with variable viscosity and thermal conductivity over a stretching surface embedded in a porous medium. Starikovicius et al. [38] used the Navier-Stokes-Brinkman system of equations to describe the coupled flow in 3D domain, consisting of fluid and porous subdomains and efficient parallel algorithms are developed to solve this problem.

A new stage in the evolution of fluid dynamics theory is in progress because of its increasing importance in the processing industries in which behaviour of the materials cannot be characterized by Newtonian relationship. Due to this reason, many non-Newtonian models or constitutive equations are proposed. Micropolar fluid obeys the constitutive equations of the considered non-Newtonian fluid model to analyze the behaviour of exotic lubricants, colloidal suspensions, polymeric fluid and liquid crystals. Eringen [15] is a pioneering researcher who has formulated the theory of micropolar fluids. This theory takes into consideration the effect of local structure and microrotations of the fluid elements. Unlike other fluids, micropolar fluid consists of microstructure belonging to a class of fluids with non-symmetrical stress tensor. Physically, it represents fluid having randomly oriented particles suspended in a porous medium. The micropolar fluid supports couple stress, body couples, micro-rotational and micro-inertial effects. The governing differential equations for micropolar fluid is highly non-linear and subtle in comparison to Newtonian fluids. A thorough review of this subject and application of micropolar fluid mechanics have been provided by Ariman et al. [8]. Vajravelu and Rollins [41] studied flow and heat transfer in viscous fluid over a nonlinearly stretching sheet without viscous dissipation, but the heat transfer in this flow is analyzed only in the case when the sheet is held at a constant temperature. Vajravelu and Hadjinicolaou [40] studied the heat transfer characteristics in a laminar boundary layer flow of viscous fluid over a linearly stretching continuous surface with viscous dissipation/frictional heating and internal heat generation. Pop et al. [33] investigated mixed convection in narrow vertical ducts without the effects of viscous dissipation. Effects of higher order chemical reaction on micropolar fluid flow on a power law permeable stretching sheet with variable concentration in a porous medium are studied by Rahman and Al-Lawatia [36].

Numerous attempts have been made to analyze the effect of transverse magnetic field on boundary layer flow characteristics by keeping in mind some specific industrial application such as polymer processing technology. Pavlov [32] and Chakrabarti and Gupta [11] analyzed the magnetohydrodynamic (MHD)

flows over a stretching sheet without and with suction, respectively by applying
the assumptions of boundary layer theory. Abo-Eldahab and El-Aziz [2] studied
the effects of blowing/suction on hydromagnetic heat transfer by mixed convec-
tion from an inclined continuously stretching surface with internal heat gener-
ation/absorption. Andersson et al. [7] solved analytically the two-dimensional
Navier–Stokes equations for the MHD fluid over a stretching sheet without ap-
plying the boundary layer theory. Makinde and Aziz [25] analyzed MHD mixed
convection from a vertical plate embedded in a porous medium by considering
convective boundary conditions. Makinde [23] investigated similarity solution
of hydromagnetic heat and mass transfer over a vertical plate with a convec-
tive surface boundary condition. Later, Makinde [22] studied MHD heat and
mass transfer over a moving vertical plate with a convective surface boundary
condition. In all the earlier studies, the effects of Ohmic heating have not been
studied by previous authors. However, it is more realistic to include this effect
to explore the impact of magnetic field on the thermal transport in the bound-
ary layer. Recently, Abo-Eldahab and El-Aziz [3] studied the effect of Ohmic
heating on mixed convection boundary layer flow of a micropolar fluid from a
rotating cone with power-law variation in surface temperature. Recently, Abel
et al. [1] studied momentum and heat transfer characteristics in an incom-
pressible electrically conducting viscoelastic boundary layer flow over a linear
stretching sheet in the presence of viscous and Ohmic dissipations.

Radiative heat transfer flow is very important in manufacturing industries
for the design of reliable equipments, nuclear plants, gas turbines and various
propulsion devices for aircraft, missiles, satellites and space vehicles. The ef-
fects of thermal radiation on the forced and free convection flows are important
in the content of space technology and processes involving high temperature.
Chamkha [12] and Chamkha and Khanafer [13] studied solar radiation assisted
free convection in the boundary layer adjacent to a vertical flat plate in a porous
medium of uniform and variable porosity. Mohammadein and El-Amin [26] an-
alyzed the thermal dispersion-radiation effects on non-Darcy natural convection
in a fluid saturated porous medium. Theoretically, a velocity square term and
a viscous term should be introduced in the momentum equations to account for
the inertia and boundary effects, respectively in the study of boundary layer
flow over the surface of a body embedded in high-porosity media. Vafai and
Tien [39] applied the Darcy–Brinkman model to study the effects of bound-
ary and inertia forces on forced convection over a fixed impermeable heated
plate embedded in a porous medium. Barletta et al. [9] presented analytical
approach to the Darcy mixed convection with viscous dissipation in a vertical
channel. In view of the industrial applications, it is interesting to examine the
flow and thermal characteristics of viscous fluid saturated in a porous media
over a stretching sheet. In the physical process of drawing a sheet from a slit
of a container, it is tacitly assumed that only the fluid adhered to the sheet
is moving but the matrix remains fixed to cope the usual assumption of flow
motion in the porous medium. Rahman [34] and Rahman and Sultana [37]
studied flow of micropolar fluid from radiate isothermal porous surfaces with
viscous dissipation and Joule heating. Recently, Makinde [24] analyzed MHD
mixed-convection interaction with thermal radiation and transverse magnetic
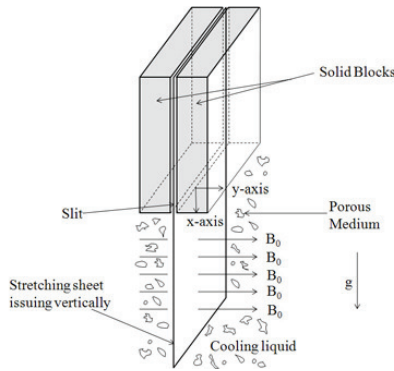
Figure 1. Physical model and coordinate system.

field past a vertical porous plate embedded in a porous medium in the presence of the n-th order chemical reaction.

The purpose of the present paper is to study the effects of thermal radiation on non-Darcian two-dimensional stagnation-point flow and heat transfer of a micropolar fluid towards a stretching sheet with Ohmic dissipation in the porous medium over a non-isothermal stretching sheet with the prescribed surface heat flux condition which is linearly proportional to the distance from the origin. The flow in a porous media deals with the analysis in which the differential equation governing the fluid motion is based on the Darcy's law which accounts for the drag exerted by the porous medium. The governing non-linear partial differential equations are transformed into a system of nonlinear ordinary differential equations and these equations are then linearized by using quasi-linearization method. The resulting linearized equations of momentum, energy and concentration equations are solved numerically using finite difference method with appropriate boundary conditions. We shall examine the effects of relevant parameters on the characteristics of flow, heat transfer and mass transfer in the present study.

2   Mathematical Formulations and Governing Equations

We consider a steady two-dimensional mixed convection flow of an incompressible, electrically conducting micropolar fluid towards a stagnation point at a surface coinciding with the plane $y = 0$ and the flow region $y > 0$. The origin is fixed as shown in Fig. 1. The x-axis is taken in the direction along which the stretching sheet is set to motion and the y-axis is taken perpendicular to it. The flow is generated by the action of two equal and opposite forces along the x-axis and the sheet is stretched in such a way that the velocity at any instant is proportional to the distance from the origin ($x = 0$). We assume that the sheet is stretched with a linear velocity $u_w = bx$, where b is a positive constant. Further the flow field is exposed to the influence of an external transverse magnetic field of strength $\vec{B} = (0, B_0, 0)$ and uniform electric field $\vec{E} = (0, 0, -E_0)$. Application of such type of electric field and magnetic field

stabilizes the boundary layer flow. The electric field $\overrightarrow{E} = (0, 0, -E_0)$ and magnetic field $\overrightarrow{B} = (0, B_0, 0)$ are satisfying the Maxwell's equations: $\nabla.\overrightarrow{B} = 0$ and $\nabla \times \overrightarrow{E} = 0$. When magnetic field is not so strong then electric field and magnetic field obey Ohm's law $\overrightarrow{J} = \sigma(\overrightarrow{E} + \overrightarrow{q} \times \overrightarrow{B})$, where $\overrightarrow{J}$ is Joule current. We have taken into account the frictional heating due to viscous dissipation since the micropolar fluid also has viscous property. With these assumptions the governing equations are given by (see Pal and Chatterjee [30]):

(i) The equation of continuity

$$\frac{\partial u}{\partial x} + \frac{\partial v}{\partial y} = 0. \tag{2.1}$$

(ii) The equation of momentum

$$u\frac{\partial u}{\partial x} + v\frac{\partial u}{\partial y} = u_\infty\frac{du_\infty}{dx} + \left(\nu + \frac{k_1^*}{\rho}\right)\frac{\partial^2 u}{\partial y^2} + \frac{k_1^*}{\rho}\frac{\partial N}{\partial y} - \frac{\nu\varphi}{k}(u - u_\infty)$$
$$- \frac{C_b}{\sqrt{k}}\varphi(u^2 - u_\infty^2) + g\beta_t(T - T_\infty) + g\beta_c(C - C_\infty)$$
$$+ \frac{\sigma}{\rho}\left(E_0B_0 - B_0^2(u - u_\infty)\right). \tag{2.2}$$

(iii) The equation of angular momentum

$$\rho j\left(u\frac{\partial N}{\partial x} + v\frac{\partial N}{\partial y}\right) = \gamma\frac{\partial^2 N}{\partial y^2} - k_1^*\left(2N + \frac{\partial u}{\partial y}\right). \tag{2.3}$$

(iv) The equation of energy

$$u\frac{\partial T}{\partial x} + v\frac{\partial T}{\partial y} = \frac{1}{\rho C_p}\frac{\partial}{\partial y}\left(\kappa\frac{\partial T}{\partial y}\right) - \frac{1}{\rho C_p}\frac{\partial q_r}{\partial y}$$
$$+ \frac{\sigma}{\rho C_p}\left((u - u_\infty)B_0 - E_0\right)^2. \tag{2.4}$$

(v) The equation of mass diffusion

$$u\frac{\partial C}{\partial x} + v\frac{\partial C}{\partial y} = D\frac{\partial^2 C}{\partial y^2}, \tag{2.5}$$

where u and v are the velocity components along the x and y directions, u_∞ is free stream velocity, ρ is the density of the liquid, φ is the porosity, k is permeability of the porous medium, β_t and β_c are the coefficients of thermal and concentration expansions respectively, T is the temperature of the fluid, C_b is the form of drag coefficient which is independent of viscosity and other properties of the fluid but depends on the geometry of the medium, E_0 is the strength of applied electric fluid, B_0 is the strength of applied magnetic fluid, g is the acceleration due to gravity, q_r is the radiative heat flux, C_p is the specific heat at constant pressure, C is concentration of the solute, D is the coefficient of

diffusivity, ν is the kinematic viscosity, σ is the electrical conductivity of the fluid, κ is the thermal conductivity, N is the component of microrotation or angular velocity whose rotation is in the direction of the x–y plane and j, γ and k_1^* are the microinertia per unit mass, spin gradient viscosity and vortex viscosity, respectively. Furthermore, the spin gradient viscosity γ, which defines the relationship between the coefficient of viscosity and micro-inertia is as follows (Kim [19]): $\gamma = \mu(1 + K/2)j$, in which $K = k_1^*/\mu$ (> 0) is the material parameter. Here all the material constants γ, μ, K, j are non-negative and we take $j = \nu/b$ as a reference length.

The appropriate physical boundary conditions for the problem under study are given by

$$u = u_w, \qquad v = 0, \qquad N = -n\frac{\partial u}{\partial y} \quad \text{at } y = 0, \tag{2.6}$$

$$u = u_\infty = ax, \qquad N \to 0 \quad \text{as } y \to \infty, \tag{2.7}$$

$$\underbrace{T = T_w = T_\infty + A_0\left(\frac{x}{l}\right)^2,}_{(PST\ case)} \qquad \underbrace{C = C_w = C_\infty + A_1\left(\frac{x}{l}\right)^2}_{(PST\ case)} \quad \text{at } y = 0, \tag{2.8}$$

$$\underbrace{-\kappa\frac{\partial T}{\partial y} = D_0\left(\frac{x}{l}\right)^2,}_{(PHF\ case)} \qquad \underbrace{-D\frac{\partial C}{\partial y} = D_1\left(\frac{x}{l}\right)^2}_{(PHF\ case)} \quad \text{at } y = 0, \tag{2.9}$$

$$T \to T_\infty, \qquad C \to C_\infty \quad \text{as } y \to \infty, \tag{2.10}$$

where l is the characteristic length, T_w is the wall temperature of the fluid and T_∞ is the temperature of the fluid far away from the sheet, C_w is the wall concentration of the solute and C_∞ is the concentration of the solute far away from the sheet. where D_0 and D_1 are constants. It should be remarked that n is a boundary parameter such that $0 \leqslant n \leqslant 1$. The case, when $n = 0$ is called strong concentration that indicates $N = 0$ near the wall represents concentrated particle flows in which the micro-elements close to the wall surface are unable to rotate (see Jena and Mathur [18]).

The case when $n = 1/2$ indicates the vanishing of anti-symmetric part of the stress tensor and denotes weak concentration whereas $n = 1$ is used for modelling of turbulent boundary layer flows (see Nazar et al. [29]). This assumption is invoked to allow the field of equations to predict the correct behaviour in the limiting case when the microstructure effects become negligible, and the microrotation N, reduces to the angular velocity which has been well established by Ahmadi [5] and Kline [20] and being used by many researchers. It is worth mentioning that the case $K = 0$ describes the classical Navier–Stokes equation for a viscous and incompressible fluid.

2.1 Similarity solutions for momentum equation and angular momentum equation

The governing Eqs. (2.2) and (2.3) admit a self-similar solution of the form

$$u = bxf'(\eta), \quad v = -\sqrt{b\nu}f(\eta), \quad \eta = \sqrt{\frac{b}{\nu}}y, \quad N = bx(b/\nu)^{1/2}g(\eta), \quad (2.11)$$

where f is the dimensionless stream function, g is the dimensionless microrotation function and η is the similarity variable. Substituting these in Eq. (2.2) we obtain the following third-order non-linear ordinary differential equation:

$$f'^2 - ff'' = \lambda^2 + (1+K)f''' - Da^{-1}(f' - \lambda) + Kg'$$
$$- \alpha(f'^2 - \lambda^2) + Ha^2(E_1 - f' + \lambda) + Gr_t h + Gr_c H, \quad (2.12)$$

where h is non-dimensional temperature, H is non-dimensional concentration, $\alpha = \frac{C_b}{b\sqrt{k}}\varphi u_w$ is local inertia coefficient parameter (Mostafa et al. [27]), $Da^{-1} = \frac{\varphi\nu}{kb}$ is inverse Darcy number, $Ha = \sqrt{\frac{\sigma}{\rho b}}B_0$ is Hartmann number, $\lambda = a/b$ is stretching sheet parameter, $E_1 = \frac{E_0}{B_0 u_w}$ is local electric parameter, $Gr_t = \frac{g\beta_t(T-T_\infty)}{b^2 l}$ is local thermal Grashof number, $Gr_c = \frac{g\beta_c(C-C_\infty)}{b^2 l}$ is local solutal Grashof number and $K = k_1^*/\mu$ is material parameter. Using the transformation (2.11), we obtain the ordinary differential equation for the function $g(\eta)$ from Eq. (2.3) as

$$f'g - fg' = (1 + K/2)g'' - K(2g + f''), \quad (2.13)$$

and the appropriate boundary conditions (2.6) and (2.7) now become

$$f(\eta) = 0, \quad f'(\eta) = 1, \quad g(\eta) = -nf''(\eta) \quad \text{at } \eta = 0,$$
$$f'(\eta) \to \lambda, \quad g(\infty) \to 0 \quad \text{as } \eta \to \infty.$$

It is worth mentioning that when $n = 1/2$, we can use $g(\eta) = -1/2f''(\eta)$ in Eq. (2.12) to obtain the following non-linear ordinary differential equation as

$$f'^2 - ff'' = \lambda^2 + (1 + K/2)f''' - Da^{-1}(f' - \lambda)$$
$$- \alpha(f'^2 - \lambda^2) + Ha^2(E_1 - f' + \lambda) + Gr_t h + Gr_c H, \quad (2.14)$$

subject to the appropriate boundary conditions

$$f(\eta) = 0, \quad f'(\eta) = 1, \quad \text{at } \eta = 0, \quad f'(\eta) \to \lambda, \quad \text{as } \eta \to \infty.$$

Since the function $g(\eta)$ does not appear in Eq. (2.14), so Eq. (2.13) is no longer required and hence Eq. (2.13) is not considered in the solution of Eq. (2.12) when $n = \frac{1}{2}$ (weak concentration). Eq. (2.14) is solved numerically for various values of the parameter λ by finite difference method. In this method we write $f' = q$ so that Eq. (2.14) becomes

$$(1 + K/2)q'' + fq' - q^2 + \lambda^2 - Da^{-1}(q - \lambda) - \alpha(q^2 - \lambda^2)$$
$$+ Ha^2(E_1 - q + \lambda) + Gr_t h + Gr_c H = 0. \quad (2.15)$$

Using Newton's linearization method (Anderson et al. [6]), the non-linear terms fq' and q^2 in Eq. (2.15) can be linearized in the following manner:

$$(fq')^{r+1} = f^r(q')^{r+1} \quad \text{and} \quad (q^{r+1})^2 = 2q^r q^{r+1} - (q^r)^2, \tag{2.16}$$

where r is the iteration level. Then q'' and q' in Eq. (2.15) are discretized using central difference scheme of second order accuracy. After linearization and discretization of the terms in Eq. (2.15) as discussed above, the discretized form of Eq. (2.15) yields a tridiagonal system of linear equations which is solved very efficiently by Thomas algorithm (Fletcher [16]).

2.2   Similarity solution of the heat and mass transfer equations

The thermal conductivity κ is assumed to vary linearly with temperature and it is of the form (Ahmad et al. [4], Pal and Mondal [31]) $\kappa = \kappa_\infty [1 + \epsilon h(\eta)]$ for PHF case, where $h(\eta) = (T - T_\infty)/(T_w - T_\infty)$, and ϵ is a small parameter. Following Rosseland approximation (Brewster [10]) the radiative heat flux q_r is modeled as,

$$q_r = -\frac{4\sigma^*}{3k^*}\frac{\partial T^4}{\partial y}, \tag{2.17}$$

where σ^* is the Stefan–Boltzmann constant and k^* is the mean absorption coefficient. Assuming that the differences in temperature within the flow are such that T^4 can be expressed as a linear combination of the temperature, we expand T^4 in Taylor's series about T_∞ as follows

$$T^4 = T_\infty^4 + 4T_\infty^3(T - T_\infty) + 6T_\infty^2(T - T_\infty)^2 + \cdots,$$

and neglecting higher order terms beyond the first degree in $(T - T_\infty)$, we get

$$T^4 \cong -3T_\infty^4 + 4T_\infty^3 T. \tag{2.18}$$

Now differentiating Eq. (2.17) w.r.t. y and using Eq. (2.18), we obtain

$$\frac{\partial q_r}{\partial y} = -\frac{16T_\infty^3 \sigma^*}{3k^*}\frac{\partial^2 T}{\partial y^2}. \tag{2.19}$$

Using Eq. (2.19) in Eq. (2.4) we obtain

$$u\frac{\partial T}{\partial x} + v\frac{\partial T}{\partial y} = \frac{1}{\rho C_p}\frac{\partial}{\partial y}\left(\left(\kappa + \frac{16T_\infty^3 \sigma^*}{3k^*}\right)\frac{\partial T}{\partial y}\right) + \frac{\sigma}{\rho C_p}\left((u - u_\infty)B_0 - E_0)\right)^2. \tag{2.20}$$

The thermal boundary conditions for solving Eq. (2.20) depend on the type of heating process considered. Now the non-dimensional temperature $h(\eta)$ and concentration $H(\eta)$ are defined in PHF case as

$$h(\eta) = \frac{T - T_\infty}{T_w - T_\infty}, \qquad H(\eta) = \frac{C - C_\infty}{C_w - C_\infty}, \tag{2.21}$$

$$T - T_\infty = \frac{D_0}{\kappa_\infty}\left(\frac{x}{l}\right)^2\sqrt{\frac{\nu}{b}}h(\eta) \quad \text{and} \quad T_w - T_\infty = \frac{D_0}{\kappa_\infty}\left(\frac{x}{l}\right)^2\sqrt{\frac{\nu}{b}}, \tag{2.22}$$

$$C - C_\infty = \frac{D_1}{\kappa_\infty}\left(\frac{x}{l}\right)\sqrt{\frac{\nu}{b}}H(\eta) \quad \text{and} \quad C_w - C_\infty = \frac{D_1}{\kappa_\infty}\left(\frac{x}{l}\right)^2\sqrt{\frac{\nu}{b}}. \tag{2.23}$$

Using Eq. (2.21) in Eq. (2.20) we obtain the non-linear ordinary differential equation for $h(\eta)$ in the form

$$(1 + Nr + \epsilon h)h'' + Pr(fh' - 2f'h) + \epsilon h'^2$$
$$+ PrHa^2 E_s \left[(f'^2 + \lambda^2 - 2\lambda f') - E_1(E_1 - 2f' + 2\lambda) \right] = 0. \qquad (2.24)$$

Using Eq. (2.21) in Eq. (2.5), we get

$$H'' + Sc(H'f - 2Hf') = 0. \qquad (2.25)$$

Corresponding thermal boundary conditions for $h(\eta)$ are given by

$$h'(\eta) = -\frac{1}{1+\epsilon}, \qquad H'(\eta) = -\frac{1}{1+\epsilon} \quad \text{at } \eta = 0,$$
$$h(\eta) \to 0, \qquad H(\eta) \to 0 \quad \text{as } \eta \to \infty. \qquad (2.26)$$

Here the prime denotes the differentiation with respect to the similarity variable η. $Pr = \frac{\mu C_p}{\kappa_\infty}$ is Prandtl number, $Nr = \frac{16\sigma^\star T_\infty^3}{3\kappa_\infty k^*}$ is thermal radiation parameter, $E_s = E_c \kappa_\infty \sqrt{\frac{b}{\nu}}$ is the scaled Eckert number, $E_c = \frac{b^2 l^2}{D_0 C_p}$ is Eckert number, $E_1 = \frac{E_0}{B_0 bx}$ is local electric parameter and $Sc = \frac{\nu}{D}$ is Schmidt number.

2.3 Skin-friction coefficient

The skin-friction coefficient, (C_f), is defined by the following relation

$$C_f = \frac{\tau_w}{\rho u_w^2/2}, \qquad (2.27)$$

where the skin-friction on the flat plate τ_w is given by

$$\tau_w = \left[(\mu + k_1^*)\frac{\partial u}{\partial y} \right]_{y=0}. \qquad (2.28)$$

Using (2.11) we obtain skin-friction coefficient from (2.27) and (2.28) as

$$C_f Re_x^{1/2} = (1 + K)f''(0),$$

where $Re_x = u_w x/\nu$ is the local Reynolds number.

3   Quasi-Linearization and Finite Difference Method

The flow Eq. (2.14) is coupled with the energy and concentration equations which is solved numerically along with Eqs. (2.24) and (2.25). The flow Eq. (2.14) constitute a nonlinear nonhomogeneous differential equation for which closed form solution cannot be obtained and hence we are required to solve the problem numerically using finite-difference approximation. A quasi-linearization technique (see Anderson et al. [6]) is first applied to replace the nonlinear terms at a linear stage. Then the implicit finite difference method is used to replace the different terms by their second-order central difference

approximations. Finally, the resulting tridiagonal system was solved using the Thomas algorithm to obtain $f(\eta)$. The energy Eqs. (2.24) and (2.25) are also non-linear second-order ordinary differential equations with variable coefficient which are also linearized by the quasi-linearization technique and then solved using implicit-finite difference method with Thomas algorithm under appropriate boundary conditions given by Eq. (2.26). The resulting system of equations has been solved in the infinite domain $0 < \eta < \infty$. Instead a finite domain in η direction can be used, with η chosen large enough which would ensure that the solutions are not affected by increasing the value of η further. The value of $\eta_\infty = 30$ was found to be adequate for all the range of physical parameters under study. To get the numerical solutions of the velocity, temperature and concentration fields a numerical code is developed. Uniform step size equal to $\Delta\eta = 0.001$ gives the converged results.

A quasi-linearization technique as described by Anderson et al. [6] is first applied to replace the nonlinear terms appearing in Eq. (2.15) to linearize in the following manner

$$
\begin{aligned}
&(q^2)^{r+1} - (fq')^{r+1} - (1 + K/2)(q'')^{r+1} + Da^{-1}(q^{r+1} - \lambda) - \lambda^2 \\
&+ \alpha\{(q^2)^{r+1} - \lambda^2\} - Ha^2\{E_1 - q^{r+1} + \lambda\} - Gr_t h^r - Gr_c H^r = 0. \quad (3.1)
\end{aligned}
$$

Now the implicit finite difference method is used to replace the second-order term by the second-order forward difference approximations and first-order term by forward difference approximation as follows

$$
q' = \frac{q_j^{r+1} - q_{j-1}^{r+1}}{\Delta\eta}, \qquad q'' = \frac{q_{j-1}^{r+1} - 2q_j^{r+1} + q_{j+1}^{r+1}}{(\Delta\eta)^2}. \quad (3.2)
$$

Using Eqs. (2.16) and (3.2) in Eq. (3.1), we get

$$
\begin{aligned}
&2q_j^r q_j^{r+1} - (q_j^r)^2 - f_j^r\left\{\frac{q_j^{r+1} - q_{j-1}^{r+1}}{\Delta\eta}\right\} + Da^{-1}\{q_j^{r+1} - \lambda\} \\
&- (1 + K/2)\left\{\frac{q_{j-1}^{r+1} - 2q_j^{r+1} + q_{j+1}^{r+1}}{(\Delta\eta)^2}\right\} - Gr_t h_j^r - Gr_c H_j^r \\
&+ \alpha\{2q_j^r q_j^{r+1} - (q_j^r)^2 - \lambda^2\} - Ha^2\{E_1 - q_j^{r+1} + \lambda\} - \lambda^2 = 0. \quad (3.3)
\end{aligned}
$$

Rearranging the terms of Eq. (3.3), we get

$$
a_j q_{j-1}^{r+1} + b_j q_j^{r+1} + c_j q_{j+1}^{r+1} = d_j, \quad 3 \le j \le n - 1, \quad (3.4)
$$

where

$$
a_j = \frac{f_j^r}{\Delta\eta} - \frac{(1 + K/2)}{(\Delta\eta)^2}, \quad b_j = 2q_j^r - \frac{f_j^r}{\Delta\eta} + 2\frac{(1 + K/2)}{(\Delta\eta)^2} + Da^{-1} + 2\alpha q_j^r + Ha^2,
$$

$$
c_j = \frac{-(1 + K/2)}{(\Delta\eta)^2}, \quad d_j = \{\lambda^2 + (q_j^r)^2\}\{1 + \alpha\} + \lambda\{Da^{-1} + Ha^2\} + Ha^2 E_1
$$

$$
+ Gr_t h_j^r + Gr_c H_j^r. \quad (3.5)
$$

When $j = 2$, we have from Eq. (3.4) as

$$b_2 q_2^{r+1} + c_2 q_3^{r+1} = d_2, \tag{3.6}$$

where

$$b_2 = 2q_2^r - \frac{f_2^r}{\Delta\eta} + 2\frac{(1+K/2)}{(\Delta\eta)^2} + Da^{-1} + 2\alpha q_2^r + Ha^2, \quad c_2 = \frac{-(1+K/2)}{(\Delta\eta)^2},$$

$$
\begin{aligned}
d_2 = {} & \left\{\lambda^2 + \left(q_2^r\right)^2\right\}\{1+\alpha\} + \lambda\left\{Da^{-1} + Ha^2\right\} + Ha^2 E_1 \\
& + Gr_t h_2^r + Gr_c H_2^r - \left\{\frac{f_2^r}{\Delta\eta} - \frac{(1+K/2)}{(\Delta\eta)^2}\right\}q_1^r.
\end{aligned}
\tag{3.7}
$$

When $j = n$, we have from Eq. (3.4) as

$$a_n q_{n-1}^{r+1} + b_n q_n^{r+1} = d_n, \tag{3.8}$$

where

$$a_n = \frac{f_n^r}{\Delta\eta} - \frac{(1+K/2)}{(\Delta\eta)^2}, \quad b_n = 2q_n^r - \frac{f_n^r}{\Delta\eta} + 2\frac{(1+K/2)}{(\Delta\eta)^2} + Da^{-1} + 2\alpha q_n^r + Ha^2,$$

$$
\begin{aligned}
d_n = {} & \left\{\lambda^2 + \left(q_n^r\right)^2\right\}\{1+\alpha\} + \lambda\left\{Da^{-1} + Ha^2\right\} + Ha^2 E_1 \\
& + Gr_t h_n^r + Gr_c H_j^n + \frac{(1+K/2)}{(\Delta\eta)^2}q_{n+1}^r.
\end{aligned}
\tag{3.9}
$$

Similarly, we can linearize the energy Eq. (2.24) by quasi-linearization technique and then the implicit finite difference method is used to replace the second-order term by second-order central difference approximations and first-order term by the central difference approximation given by

$$h' = \frac{h_{j+1}^{r+1} - h_{j-1}^{r+1}}{2\Delta\eta}, \qquad h'' = \frac{h_{j-1}^{r+1} - 2h_j^{r+1} + h_{j+1}^{r+1}}{(\Delta\eta)^2}. \tag{3.10}$$

Thus from Eq. (2.24) takes the following form

$$\alpha_j h_{j-1}^{r+1} + \beta_j h_j^{r+1} + \gamma_j h_{j+1}^{r+1} = \lambda_j, \quad 3 \le j \le n-1, \tag{3.11}$$

where

$$\alpha_j = \frac{1+Nr}{(\Delta\eta)^2} - \frac{Pr f_j^r}{2\Delta\eta} + \frac{\epsilon h_j^r}{(\Delta\eta)^2} - \frac{\epsilon(h_{j+1}^r - h_{j-1}^r)}{2(\Delta\eta)^2}, \tag{3.12}$$

$$\beta_j = -2Pr q_j^r - \frac{2(1+Nr)}{(\Delta\eta)^2} - \frac{2\epsilon h_j^r}{(\Delta\eta)^2},$$

$$\gamma_j = \frac{1+Nr+\epsilon h_j^r}{(\Delta\eta)^2} + \frac{Pr f_j^r}{2\Delta\eta} + \frac{\epsilon(h_{j+1}^r - h_{j-1}^r)}{2(\Delta\eta)^2},$$

$$\lambda_j = \frac{\epsilon(h_{j+1}^r - h_{j-1}^r)^2}{4(\Delta\eta)^2} - Pr Ha^2 E_s\left[\left((q_j^r)^2 + \lambda^2 - 2\lambda q_j^r\right) + E_1\left(E_1 - 2q_j^r + 2\lambda\right)\right].$$

When $j = 2$, we have from Eq. (3.11) as

$$\beta_2 h_2^{r+1} + \gamma_2 h_3^{r+1} = \lambda_2, \tag{3.13}$$

where

$$\beta_2 = -2Prq_2^r - \frac{2(1 + Nr)}{(\Delta\eta)^2} - \frac{2\epsilon h_2^r}{(\Delta\eta)^2}, \quad \gamma_2 = \frac{2(1 + Nr + \epsilon h_2^r)}{(\Delta\eta)^2},$$

$$\lambda_2 = -\frac{2(1 + Nr + \epsilon h_2^r)}{\Delta\eta(1 + \epsilon)} + \frac{Prf_2^r}{(1 + \epsilon)} + \frac{\epsilon(h_3^r - h_1^r)}{\Delta\eta(1 + \epsilon)} + \frac{\epsilon(h_3^r - h_1^r)^2}{4(\Delta\eta)^2}$$
$$- PrHa^2 E_s\left[\left((q_2^r)^2 + \lambda^2 - 2\lambda q_2^r\right) + E_1\left(E_1 - 2q_2^r + 2\lambda\right)\right]. \tag{3.14}$$

When j=n, we have from Eq. (3.11) as

$$\alpha_n h_{n-1}^{r+1} + \beta_n h_n^{r+1} = \lambda_n, \tag{3.15}$$

where

$$\alpha_n = \frac{1 + Nr + \epsilon h_n^r}{(\Delta\eta)^2} - \frac{Prf_n^r}{2\Delta\eta} - \frac{\epsilon(h_{n+1}^r - h_{n-1}^r)}{2(\Delta\eta)^2},$$

$$\beta_n = -2Prq_n^r - \frac{2(1 + Nr + \epsilon h_n^r)}{(\Delta\eta)^2},$$

$$\lambda_n = \frac{\epsilon(h_{n+1}^r - h_{n-1}^r)^2}{4(\Delta\eta)^2} - PrHa^2 E_s\left[\left((q_n^r)^2 + \lambda^2 - 2\lambda q_n^r\right) + E_1\left(E_1 - 2q_n^r + 2\lambda\right)\right]$$
$$- \left[\frac{1 + Nr + \epsilon h_n^r}{(\Delta\eta)^2} + \frac{Prf_n^r}{2\Delta\eta} + \frac{\epsilon(h_{n+1}^r - h_{n-1}^r)}{2(\Delta\eta)^2}\right]h_{n+1}^r.$$

Similar procedure is adopted for the concentration Eq. (2.25) using quasi-linearization and central difference method as discussed above, so we obtain

$$A_j H_{j-1}^{r+1} + B_j H_j^{r+1} + C_j H_{j+1}^{r+1} = D_j \quad (3 \leq j \leq n - 1) \tag{3.16}$$

where

$$A_j = \frac{1}{(\Delta\eta)^2} - \frac{Scf_j^r}{2\Delta\eta}, \quad B_j = -\frac{2}{(\Delta\eta)^2} - 2Scq_j^r,$$

$$C_j = \frac{1}{(\Delta\eta)^2} + \frac{Scf_j^r}{2\Delta\eta}, \quad D_j = 0. \tag{3.17}$$

When $j = 2$, we have from Eq. (3.16) as

$$B_2 H_2^{r+1} + C_2 H_3^{r+1} = D_2, \tag{3.18}$$

where

$$B_2 = -\frac{2}{(\Delta\eta)^2} - 2Scq_2^r, \quad C_2 = \frac{2}{(\Delta\eta)^2}, \quad D_2 = \frac{2Scf_2^r}{(1 + \epsilon)} - \frac{2}{\Delta\eta(1 + \epsilon)}. \tag{3.19}$$

When $j = n$, we have from Eq. (3.16) as

$$A_n H_{n-1}^{r+1} + B_n H_n^{r+1} = D_n, \tag{3.20}$$

where

$$A_n = \frac{1}{(\Delta\eta)^2} - \frac{Scf_n^r}{2\Delta\eta}, \ B_n = -\frac{2}{(\Delta\eta)^2} - 2Scq_n^r, \ D_n = -\left[\frac{1}{(\Delta\eta)^2} + \frac{Scf_n^r}{2\Delta\eta}\right]H_{n+1}^r.$$

The system of linear Eqs. (3.4)–(3.20) are solved very efficiently by Thomas algorithm for the unknowns.

4   Discussion of the Results

Present results of the dimensionless skin friction coefficient $f''(0)$, temperature profile $h(0)$ and concentration profile $H(0)$ are compared with those obtained by Andersson et al. [7] and Chen [14] and excellent agreement has been obtained as seen from Table 1. This indicates the accuracy and correctness of the numerical results obtained and also validates the numerical code developed using quasi-linearization with finite-difference technique. A comparison of numerical results of skin-friction coefficient with Mahapatra and Gupta [21] and Nazar et al. [28] are made in Table 2, for PST case.

Table 1.   Comparison of skin friction coefficient $C_f Re_x^{\frac{1}{2}}$ for $K = 0$, $Sc = 0.22$ (Newtonian fluid).

Ha	Andersson et al. [7]	Chen [14]	Present result (PHF case)
0.0	1.00	1.00	1.00
1.0	1.414	1.41421	1.41420
1.5	1.581	1.58114	1.57485
2.0	1.732	1.73205	1.73252

Table 2.   Comparison of skin-friction coefficient for PST case (Newtonian fluid).

λ	Mahapatra and Gupta [21]	Nazar et al. [28]	Present results (PST case)
0.01		−0.9980	−0.99670
0.2	−0.9181	−0.9181	−0.91921
0.5	−0.6673	−0.6673	−0.66732
1.0		0.0	0.0
2.0	2.0175	2.0175	2.01729
5.0		11.7537	11.75029
10.0		36.2687	36.25047
20.0		106.5744	106.4931

The effect of magnetic field, electric field, thermal radiation and inverse Darcy number on skin friction coefficient $f''(0)$, temperature profile $h(0)$ and concentration profile $H(0)$ for PHF cases are tabulated in Table 3, when $\lambda = 0.5$, $K = 0.2$, $n = 0.5$, $E_s = 0.05$, $Gr_t = 0.2$, $Gr_c = 0.1$, $Pr = 0.71$, $\epsilon = 0.01$, $Sc = 0.22$, $\alpha = 0.1$. It is seen from this table that the effect of magnetic

Table 3. Values of skin friction coefficient $f''(0)$, surface temperature $h(0)$ and surface concentration $H(0)$.

Ha	E_1	Nr	Da^{-1}	$f''(0)$	$h(0)$	$H(0)$
1.0	0.1	0.2	2.0	-0.66694	0.93462	1.75039
1.5				-0.77418	0.94326	1.76045
2.0				-0.90492	0.95336	1.77332
0.1	0.5	0.2	2.0	-0.57007	0.92695	1.74385
	1.0			-0.56661	0.92644	1.74178
	1.5			-0.56319	0.92608	1.73971
0.1	0.1	1.0	2.0	-0.52802	1.33411	1.72849
		2.0		-0.49170	1.64626	1.71383
		3.0		-0.46049	1.90773	1.70100
0.1	0.1	0.2	0.5	-0.78703	0.95082	1.79312
			1.0	-0.65114	0.93636	0.17640
			2.0	-0.57279	0.92749	1.74551

Table 4. Calculation of absolute error for $f''(0)$, $h(0)$, $H(0)$.

Ha		$\eta = 5$ (i)	$\eta = 10$ (ii)	$\eta = 20$ (iii)	$\eta = 30$ (iv)	Percentage $[(iv) - (iii)/(iv)]$
1.5	$f''(0)$	-0.78957	-0.78880	-0.77781	-0.77718	0.08106
	$h(0)$	0.93049	0.93913	0.94284	0.94326	0.25656
	$H(0)$	1.74589	1.75434	1.75987	1.76045	0.03295
2.5	$f''(0)$	-0.92325	-0.92050	-0.91098	-0.91080	0.01976
	$h(0)$	0.94089	0.94343	0.95006	0.95336	0.34614
	$H(0)$	1.75876	1.76545	1.77332	1.77389	0.03213

Table 5. Grid-invariance test for velocity profile.

η_∞	η	$\Delta\eta = 0.04$	$\Delta\eta = 0.02$	$\Delta\eta = 0.01$
10	0.6	0.74596	0.74403	0.74191
	1.0	0.65401	0.65209	0.64998
	2.0	0.55301	0.55195	0.55080
20	0.6	0.74598	0.74405	0.74193
	1.0	0.65404	0.65212	0.65006
	2.0	0.55308	0.55201	0.55086

field is to increase $h(0)$ and $H(0)$ whereas reverse effect is seen for skin friction coefficient $f''(0)$. The effect of electric field is to decrease $h(0)$ and $H(0)$, whereas reverse trend is observed on $f''(0)$. Table 3 also shows the effect of thermal radiation on $f''(0)$, $h(0)$ and $H(0)$. It is seen from this table that the effect of increasing the value of Nr is to increase the value of $f''(0)$ and $h(0)$ whereas its effect is to decrease the value of $H(0)$. By analyzing this table it is found that the effect of inverse Darcy number Da^{-1} is to decrease the values of $f''(0)$ whereas opposite effects are seen for $h(0)$ and $H(0)$. In

Table 6.   Grid-invariance test for temperature profile.

η_∞	η	$\Delta\eta = 0.04$	$\Delta\eta = 0.02$	$\Delta\eta = 0.01$
10	0.6	0.46310	0.43807	0.40618
	1.0	0.33189	0.30114	0.26561
	2.0	0.13613	0.12368	0.10920
20	0.6	0.46309	0.43800	0.40618
	1.0	0.33188	0.30113	0.26560
	2.0	0.13611	0.12363	0.10918

Table 7.   Grid-invariance test for concentration profile.

η_∞	η	$\Delta\eta = 0.04$	$\Delta\eta = 0.02$	$\Delta\eta = 0.01$
10	0.6	1.29098	1.27349	1.26632
	1.0	1.05221	1.03865	1.03270
	2.0	0.64399	0.63607	0.63273
20	0.6	1.29115	1.27413	1.26648
	1.0	1.05240	1.03883	1.03289
	2.0	0.64428	0.63635	0.63301
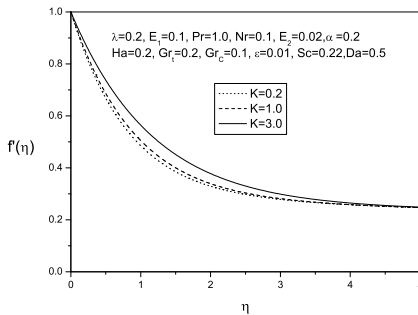
Figure 2.   Variation of velocity profiles f' with η for different values of K.
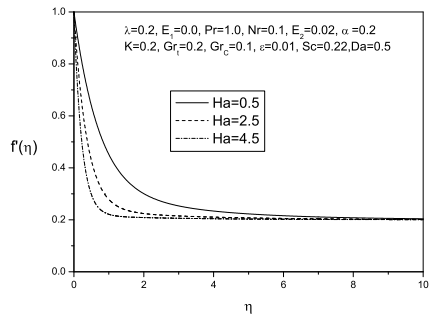
Figure 3.   Variation of velocity profiles f' with η for different values of Ha.

all the tables from 4–7 and figures we have considered $n = 0.5$. Table 4, represents the different values of skin friction coefficient $f''(0)$, temperature and concentration profiles for different values of Hartmann number. Here it is seen that the percentage error is very negligible for skin friction coefficient, temperature profile $h(0)$ and concentration profile $H(0)$. So from our findings we can say that our numerical technique adopted in this paper is very efficient. In Table 5, different values of velocity distributions are provided for different grid sizes, in order to have a clear picture of the grid convergence. Thus it is seen that the values of velocity distribution $f'(\eta)$ have very small changes when the grid size is reduced for different values of η_∞. Accordingly the similar findings are recorded for temperature and concentration profiles in Table 6 and Table 7.
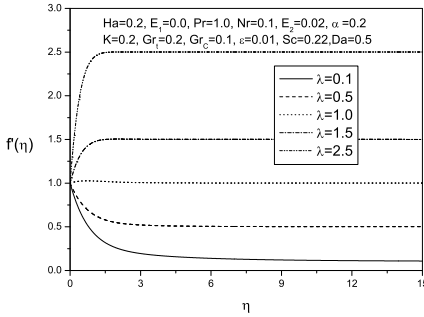
Figure 4. Variation of velocity profiles f' with η for different values of λ.
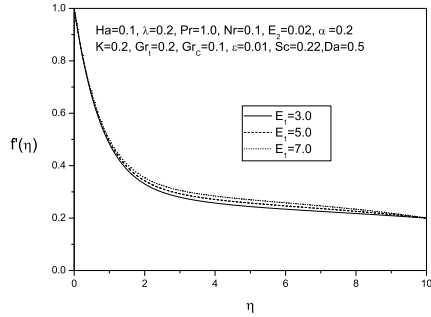
Figure 5. Variation of velocity profiles f' with η for different values of E_1.

In this section the influence of emerging physical parameters on velocity, temperature and concentration profiles are shown graphically in Figs. 2–11. Profiles for velocity distributions are plotted in Figs. 2–5. These results illustrate the influence of various physical parameters on velocity profiles. The values of $f''(0)$, $h(0)$ and $H(0)$ have been checked with different values of η_∞ and those values are chosen which gave no further changes in the values of $f''(0)$, $h(0)$ and $H(0)$ up to six decimal places. Hence the scheme used in this paper is found to be suitable and accurate. Fig. 2 is plotted to discuss the behaviour of velocity profiles for different values of material parameters K. It is clear from this figure that an increase in the value of K leads to an increase of the velocity profile. Fig. 3 displays results for the effect of velocity profile for various values of the Hartmann number Ha. It is clearly observed from this figure that the velocity profile decreases with increase in the value of the Hartmann number. It is well known that the Hartmann number represents the importance of magnetic field on the flow. The transverse magnetic field sets a Lorentz force which results in retarding force on the velocity field. Hence, when the Hartmann number increases the Lorentz force also increases due to which velocity profiles decrease.

Fig. 4 is a plot of the variation of velocity profile for various values of λ in the boundary layer. It can be clearly seen from this figure that the velocity profile decreases till it matches the boundary condition at $\eta = \infty$ when $\lambda = 0.1, 0.5$, whereas when $\lambda > 1$, the velocity profile increases and becomes constant far away from the stretching sheet. Fig. 5 shows the velocity profiles for various values of local electric field parameter. We note here that the presence of local electric field parameter enhances the velocity in the boundary layer. The analysis of the graph further reveals that the effect of local electric parameter E_1 is more prominently visible near the stretching boundary layer because Lorentz force arising due to electric field acts as an accelerating force in reducing fractional resistance which causes the velocity field to increase with electric field. This figure also shows an exponential decrease in the velocity profile till it satisfies the boundary condition at infinity.

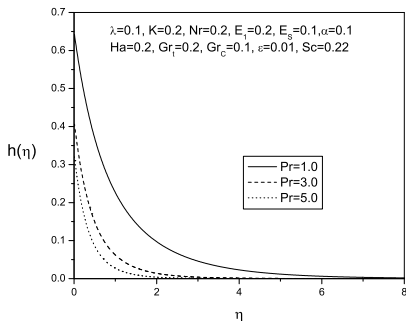Fig. 6 illustrates the variation of temperature profiles for various values of

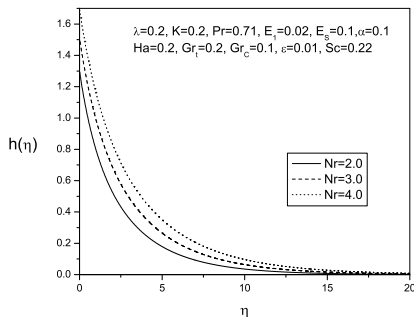**Figure 6.** Variation of temperature profiles with η for different values of Pr.

Figure 7. Plot of temperature profiles with η for different values of Nr.
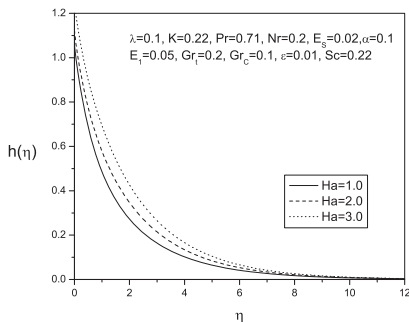

Figure 8. Variation of temperature profiles with η for different values of Ha.
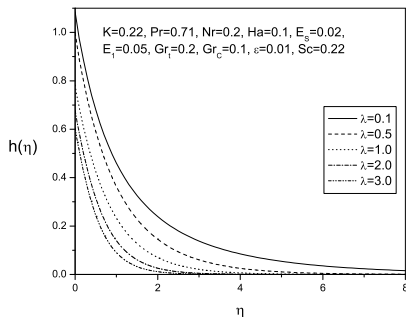

Figure 9. Variation of temperature profiles with η for different values of λ.

Prandtl number. From this figure it is seen that the temperature decreases with increasing the values of Prandtl number Pr in the boundary layer. From this plot, it is evident that temperature in the boundary layer falls very quickly for large value of the Prandtl number because thickness of the boundary layer decreases with increase in the value of the Prandtl number. Fig. 7 represents the temperature profiles for various values of thermal radiation parameter Nr. This figure indicates that the effect of thermal radiation is to enhance heat transfer because of the fact that thermal boundary layer thickness increases with increase in the thermal radiation parameter. Thus it is pointed out that the radiation should be minimized to have the cooling process at a faster rate. Fig. 8 depicts the effect of Hartmann number Ha on temperature profile. It is observed from this plot that the temperature increases with increasing the value of Hartmann number. Further, it is noted that the thermal boundary layer thickness increases in the presence of transverse magnetic field. The reason behind increase of temperature in the thermal boundary layer depends on the fact that a body force (called Lorentz force) is produced which opposes the motion in the presence of transverse magnetic field and the resistance offered to the flow is responsible for increasing the temperature.
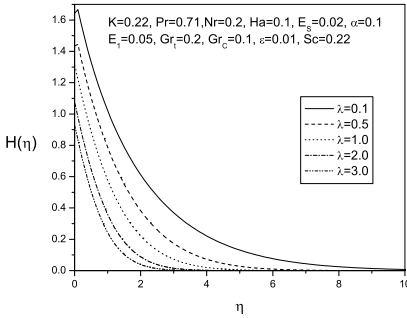
Figure 10. Variation of concentration profiles with η for different values of λ.
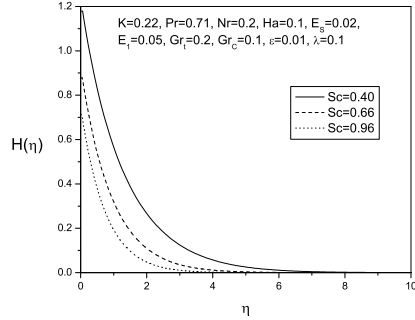
Figure 11. Variation of concentration profiles with η for different values of Sc and $\alpha = 0.1$.

Fig. 9 shows the variation of temperature $h(\eta)$ with η for several values of λ. It is seen from this figure that the effect of λ is to reduce the temperature in the thermal boundary layer which is due to the fact that increase in λ reduces the thermal boundary layer thickness. The reduction in the thermal boundary layer thickness in PHF case shows that it takes less time for cooling the stretching sheet for large values of λ. Fig. 10 is the plot of concentration distribution for various values of λ. As observed from this figure that concentration decreases with increase in the value of λ due to the fact that increase in λ causes thinning of the solutal boundary layer thickness. Similar effect is seen in Fig. 11 for the increase in the value of Schmidt number Sc.

5 Conclusions

The present paper deals with analyzing the effect of thermal radiation on MHD heat and mass transfer of a micropolar fluid near a stagnation point towards a stretching surface with ohmic dissipation and prescribed heat flux. The governing boundary layer non-linear differential equations are solved numerically by finite-difference method using quasi-linearization technique. Based on the results and discussion section, following conclusions are drawn:

(i) The velocity increases with the increase in the value of Electric field parameter E_1, material parameter K and stretching sheet parameter λ but reverse trend is seen by increasing the Hartmann number Ha in PHF case.

(ii) The temperature decreases as there is increase in the value of Prandtl number whereas opposite effect is seen by enhancing the value of thermal radiation and magnetic field when stretching sheet parameter $\lambda = 0.1$.

(iii) The concentration decreases with increase of the value of the Schmidt number Sc and stretching sheet parameter λ.

(iv) The skin friction coefficient decreases with increase in the value of Hartmann number whereas reverse trend is seen with increase in λ, Electric field, E_1 and thermal radiation parameter Nr.

References

[1] M.S. Abel, E. Sanjayanand and M.M. Nandeppanavar. Viscoelastic MHD flow and heat transfer over a stretching sheet with viscous and Ohmic dissipation. *Comm. Nonlinear Sci. Numer. Simul.*, **13**:1808–1821, 2008. http://dx.doi.org/10.1016/j.cnsns.2007.04.007.

[2] E.M. Abo-Eldahab and M.A. El-Aziz. Blowing/suction effect on hydromagnetic heat transfer by mixed convection from an inclienol continuously stretching sheet with internal heat generation/absorption. *Int. J. Thermal. Sci.*, **43**:709–719, 2004. http://dx.doi.org/10.1016/j.ijthermalsci.2004.01.005.

[3] E.M. Abo-Eldahab and M.A. El-Aziz. Hall current and ohmic heating effect on mixed convection boundary layer flow of a micropolar fluid from a rotating cone with power-law variation in surface temperature. *Int. Comm. Heat Mass Transfer*, **31**:751–762, 2004. http://dx.doi.org/10.1016/S0735-1933(04)00062-4.

[4] N. Ahmad, Z. Siddiqui and M.K. Mishra. Boundary layer flow and heat transfer past a stretching plate with variable thermal conductivity. *Int. J. Nonlinear Mech.*, **45**:306–309, 2010. http://dx.doi.org/10.1016/j.ijnonlinmec.2009.12.006.

[5] G. Ahmadi. Self similar solution of incompressible micropolar boundary layer flow over a semi-infinite flat plate. *Int. J. Eng. Sci.*, **14**:639–646, 1976. http://dx.doi.org/10.1016/0020-7225(76)90006-9.

[6] D.A. Anderson, J.C. Tannehill and R.H. Pletcher. *Computational Fluid Mechanics and Heat Transfer*. McGraw Hill Book Company, New York, NY, 1984.

[7] H.I. Andersson, K.H. Bech and B.S. Dandapat. Magnetohydrodynamic flow of a power-law fluid over a stretching sheet. *Int. J. Non-Linear Mech.*, **27**:929–936, 1992. http://dx.doi.org/10.1016/0020-7462(92)90045-9.

[8] T. Ariman, M.A. Turk and N.D. Sylvester. Microcontinuum fluids mechanics – A review. *Int. J. Eng. Sci.*, **11**:905–930, 1973. http://dx.doi.org/10.1016/0020-7225(73)90038-4.

[9] A. Barletta, E. Magyari, I. Pop and L. Storesletten. Unified analytical approch to the Darcy mixed convection with viscous dissipation in a vertical channel. *Int. J. Thermal Sci.*, **47**:408–416, 2008. http://dx.doi.org/10.1016/j.ijthermalsci.2007.03.014.

[10] M.Q. Brewster. *Thermal Radiative Transfer Properties*. John Kliley and Sons, 1972.

[11] A. Chakrabarti and A.S. Gupta. Hydromagnetic flow and heat transfer over a stretching sheet. *Quart. Appl. Math.*, **37**:73–78, 1979.

[12] A.J. Chamkha. Solar radiation assisted convection in uniform porous medium supported by a vertical flat plate. *ASME J. Heat Transfer*, **119**:89–96, 1997. http://dx.doi.org/10.1115/1.2824104.

[13] A.J. Chamkha and K. Khanafer. Nonsimilar combined convection flow over a vertical surface embedded in a variable porosity medium. *J. Porous Media*, **2**:231–249, 1999.

[14] C.-H. Chen. Effects of magnetic field and suction/injection on convection heat transfer of non-newtonian power-law fluids past a power law stretching sheet with surface heat flux. *Int. J. Thermal Sci.*, **47**:954–961, 2007. http://dx.doi.org/10.1016/j.ijthermalsci.2007.06.003.

[15] A.C. Eringen. Theory of micropolar fluids. *J. Math. Mech.*, **16**:1–18, 1966.

[16] C.A.J. Fletcher. *Computational Technique for Fluid Dynamics*. Springer-Verlag, New York, NY, 1988.

[17] P.S. Gupta and A.S. Gupta. Heat and mass transfer on a stretching sheet with suction or blowing. *Canad. J. Chem. Engg.*, **55**:744–746, 1977. http://dx.doi.org/10.1002/cjce.5450550619.

[18] S.K. Jena and M.N. Mathur. Similarity solutions for laminar free convection flow of a thermo-micropolar fluid past a nonisothermal flat plate. *Int. J. Eng. Sci.*, **19**:1431–1439, 1981. http://dx.doi.org/10.1016/0020-7225(81)90040-9.

[19] Y.J. Kim. Thermal boundary layer flow of a micropolar fluids past a wedge with constant wall temperature. *Acta Mech.*, **138**:113–121, 1999. http://dx.doi.org/10.1007/BF01179545.

[20] K. Kline. A spin velocity relation for unidirectional plane flows of micropolar fluids. *Int. J. Eng. Sci.*, **15**:131–134, 1977. http://dx.doi.org/10.1016/0020-7225(77)90028-3.

[21] T.R. Mahapatra and A.S. Gupta. Heat transfer in stagnation-point flow towards a stretching sheet. *Heat Mass Trans.*, **38**:517–521, 2002. http://dx.doi.org/10.1007/s002310100215.

[22] O.D. Makinde. On mhd heat and mass transfer over a moving vertical plate with a convective surface boundary condition. *Canad. J. Chem. Engg.*, **88**:983–990, 2010. http://dx.doi.org/10.1002/cjce.20369.

[23] O.D. Makinde. Similarity solution of hydromagnetic heat and mass transfer over a vertical plate with a convective surface boundary condition. *Int. J. Physical Sci.*, **5**(6):700–710, 2010.

[24] O.D. Makinde. Mhd mixed-convection interaction with thermal radiation and nth order chemical reaction past a vertical porous plate embedded in a porous medium. *Chem. Engg. Commun.*, **198**(4):590–608, 2011. http://dx.doi.org/10.1080/00986445.2010.500151.

[25] O.D. Makinde and A. Aziz. Mhd mixed convection from a vertical plate embedded in a porous medium with a convective boundary condition. *Int. J. Thermal Sci.*, **49**:1813–1820, 2010. http://dx.doi.org/10.1016/j.ijthermalsci.2010.05.015.

[26] A.A. Mohammadein and M.F. El-Amin. Thermal dispersion-radiation effects on non-Darcy natural convection in a fluid saturated porous medium. *Transport Porous Medium*, **40**:153–163, 2000. http://dx.doi.org/10.1023/A:1006654309980.

[27] A.A. Mostafa, A.-E. Mahmoud and S.E. Waheed. Hydromagnetic boundary layer micropolar fluid flow over a stretching surface embedded in a non-Darcian porous medium with radiation. *Mathemetical Problems in Engineering Article*, pp. 1–10, 2006. http://dx.doi.org/10.1155/MPE/2006/39392. Article ID 39392

[28] R. Nazar, N. Amin, D. Filip and I. Pop. Stagnation-point flow of a micropolar fluid towards a stretching sheet. *Int. J. Nonlin. Mech.*, **39**:1227–1235, 2004. http://dx.doi.org/10.1016/j.ijnonlinmec.2003.08.007.

[29] R. Nazar, N. Amin and I. Pop. Mixed convection boundary layer flow from a horizontal circular cylinder in micropolar fluids case of constant wall temperature. *Int. J. Numer. Methods Heat Fluid Flow*, **13**:86–109, 2003. http://dx.doi.org/10.1108/09615530310456778.

[30] D. Pal and S. Chatterjee. Heat and mass transfer in mhd non-darcian flow of a micropolar fluid over a stretching sheet embedded in a porous media with non-uniform heat source and thermal radiation. *Commun. Nonlinear Sci. Numer. Simulat.*, **15**:1843–1857, 2010. http://dx.doi.org/10.1016/j.cnsns.2009.07.024.

[31] D. Pal and H. Mondal. Mhd non-darcian mixed convection heat and mass transfer over a non-linear stretching sheet with soret–dufour effects and chemical reaction. *Int. Comm. Heat Mass Transfer*, **38**:463–467, 2011. http://dx.doi.org/10.1016/j.icheatmasstransfer.2010.12.039.

[32] K.B. Pavlov. Magnetohydrodynamic flow of an incompressible viscous fluid caused by deformation of a plane surface. *Magnitnaya Gidrodinamika*, **4**:146–147, 1974.

[33] I. Pop, D.A.S. Rees and C. Egbers. Mixed convection flow in a narrow vertical duct filled with a porous medium. *Int. J. Thermal. Sci.*, **43**:489–498, 2004. http://dx.doi.org/10.1016/j.ijthermalsci.2003.09.004.

[34] M.M. Rahman. Convective flow of micropolar fluids from radiate isothermal porous surfaces with viscous dissipation and joule heating. *Commun. Nonlinear Sci. Numer. Simulat.*, **14**(7):3018–3030, 2009. http://dx.doi.org/10.1016/j.cnsns.2008.11.010.

[35] M.M. Rahman. Combined effects of internal heat generation and higher order chemical reaction on the non-Darcian forced convective flow of a viscous incompressible fluid with variable viscosity and thermal conductivity over a stretching surface embedded in a porous medium. *Canad. J. Chem. Engg.*, 2011. http://dx.doi.org/10.1002/cjce.20644.

[36] M.M. Rahman and M. AL-Lawatia. Effects of higher order chemical reaction on micropolar fluid flow on a power law permeable stretching sheet with variable concentration in a porous medium. *Canad. J. Chem. Engg.*, **88**:23–32, 2010. http://dx.doi.org/10.1002/cjce.20244.

[37] M.M. Rahman and T. Sultana. Radiative heat transfer flow of micropolar fluid with variable heat flux in a porous medium. *Nonlinear Anal. Model. Control*, **13**(1):71–87, 2008.

[38] V. Starikovičius, R. Čiegis and O. Iliev. A parallel solver for design of oil filters. *Math. Model. Anal.*, **16**(2):326–342, 2011. http://dx.doi.org/10.3846/13926292.2011.582591.

[39] K. Vafai and C.L. Tien. Boundary and inertia effects on flow and heat transfer in porous media. *Int. J. Heat Mass Transfer*, **24**:195–203, 1981. http://dx.doi.org/10.1016/0017-9310(81)90027-2.

[40] K. Vajravelu and A. Hadjinicolaou. Heat transfer in a viscous fluid over a stretching sheet with viscous dissipation and internal heat generation. *Int. Comm. Heat Mass Transfer*, **20**:417–430, 1993. http://dx.doi.org/10.1016/0735-1933(93)90026-R.

[41] K. Vajravelu and D. Rollins. Heat transfer in electrically conducting fluid over a stretching sheet. *Int. J. Non-Linear Mech.*, **27**:265–277, 1992. http://dx.doi.org/10.1016/0020-7462(92)90085-L.